*Near Surface Geophysics, 2003, 57-67*

# Assessing reliability of 2D resistivity imaging in mountain permafrost studies using the depth of investigation index method

L. Marescot[1,3*], M.H. Loke[2], D. Chapellier[1], R. Delaloye[5], C. Lambiel[4] and E. Reynard[4]

[1]*Institute of Geophysics, University of Lausanne, 1015 Lausanne, Switzerland*
[2]*School of Physics, Universiti Sains Malaysia, 11800 Penang, Malaysia*
[3]*Laboratoire Central des Ponts et Chaussées, 44341 Bouguenais, France*
[4]*Institute of Geography, University of Lausanne, 1015 Lausanne, Switzerland*
[5]*Department of Geosciences, Geography, University of Fribourg, 1700 Fribourg, Switzerland*

Received February 2002, revision accepted November 2002

**ABSTRACT**

2D electrical resistivity tomography has been applied within a mountain permafrost environment to assist in ice location. In the context of climate change, a warming process could partially thaw this permafrost and thereby increase the risk of slope instabilities. The extent and location of permafrost are therefore of considerable interest to civil engineers.

The most challenging aspect of resistivity surveys on mountain permafrost concerns the surface layer, which mainly consists of large blocks with air voids. To overcome the very poor electrical contact, long steel stakes and sponges soaked in salt water are used as electrodes. Nevertheless, only a weak current can be injected. Another challenging aspect is the high resistivity contrast between frozen and unfrozen material, which makes inversion and interpretation difficult and problematic. In order to assess whether features at depth, indicated by the data, are real or are artefacts of the inversion process, a special inversion algorithm was applied to process depth of investigation (DOI) index maps. This method carries out two inversions of the same data set using different values of the reference resistivity. The two inversions give the same resistivity values in areas where the data contain information about the resistivity of the subsurface. On the other hand, the final result depends on the reference resistivity in areas where the data do not constrain the model.

As can be deduced from field data from the Swiss Alps and the Jura Mountains, this methodology prevents over-interpretations or misinterpretations of inversion results in mountain permafrost studies. From the DOI calculations, it is evident that little reliable information on the bedrock under the massive ice can be obtained and that the resistivity within the high resistivity zones cannot be determined accurately. The DOI map also helps to explain the occurrence of erratic and non-geological structures at depth and indicates to what depth an inverted resistivity profile can provide results.

## INTRODUCTION

There is increasing concern about mountain permafrost in the context of climate change (Haeberli *et al.* 1993). A warming process could partially thaw the permafrost and thereby increase the risk of slope instabilities such as landslides or mud flows (Haeberli *et al.* 1999). Therefore, the extent and location of permafrost and ground ice are of considerable interest to civil engineers because of construction work (ski resort buildings, cable-car poles) and other geotechnical and land-management activities in mountain areas (Haeberli 1992; Harris *et al.* 2001). Most geological material with ice content has a higher electrical resistivity than the surrounding unfrozen material. Thus, electrical imaging could prove useful in giving information about the subsurface lithology. This method is increasingly

* laurent.marescot@ig.unil.ch

used in mountain permafrost studies (see for example Hauck and Vonder Mühll 1999; Kneisel *et al.* 2000; Hauck 2001; Marescot *et al.* 2001; Vonder Mühll *et al.* 2001) but still needs a methodology to quantify the confidence we can have in the existence of features in the models at depth.

The most challenging aspect of this kind of study concerns the difficult survey conditions. The research areas usually have significant topographic variations and the surface layer consists mainly of large blocks with huge air voids (typically 1 $m^3$) and no real soil. In the present work, 2D electrical resistivity imaging surveys were conducted to provide reliable information on the distribution of ground ice in areas with very poor electrical contact, using an appropriate electrode device.

Besides this data acquisition problem, another challenging aspect is the high resistivity contrast at depth, which can vary from less than 1 kΩm to several MΩm. Layers deeper than the resistive permafrost may not have sufficient influence on the data, thus making interpretation at depth difficult, non-representative and dangerous. To assess whether features at depth, indicated by the data, are real or are artefacts of the inversion process, we need to quantify the depth of investigation of the survey. The most traditional approaches use computation of the maximum signal at depth (Roy and Apparao 1971; Roy 1972) or the median depth of investigation (Edwards 1977) for a homogeneous medium. These approaches have been summarized by Barker (1989). In a subsurface with heterogeneous high-resistivity features, these methods cannot be applied to quantify the depth of investigation. Our approach is to use depth of investigation (DOI) index calculations to determine the depth below which the data are no longer sensitive to the physical properties of the subsurface (Oldenburg and Li 1999).

This paper first reviews the general geomorphological features of permafrost in unconsolidated terrains. The next section describes the methodology developed for the surveys. Finally, the inversion and DOI index algorithms are outlined and field data from the Swiss Alps and Jura Mountains are inverted and presented with their DOI index maps. The research sites (Fig. 1) are located in the Verbier area (western Swiss Alps, 2400 m to 2800 m a.s.l.) and in the Jura Mountains (Creux du Van, north-western Switzerland, 1200 m a.s.l.).


FIGURE 1
Locations of the research sites: the Verbier (Swiss Alps) and Creux du Van (Jura Mountains) areas.

## GEOLOGICAL SETTING

Permafrost, which is defined as a subsurface material with temperature permanently lower than 0°C, is likely to be met above an elevation of roughly 2300 m in the Swiss Alps, although it can conceivably be encountered at lower altitudes. Rock glaciers are typical landforms indicating the presence of discontinous/continuous permafrost (Barsch 1996). On the other hand, sporadic patches of permafrost usually occur without the associated creeping characteristic. Frozen ground is also to be expected where historical margins of retreating glaciers are located in the potential belt of permafrost (Maisch *et al.* 1999; Kneisel 1999; Delaloye and Devaud 2000).

A schematic stratigraphic model for alpine permafrost terrain can be described as follows. The subsurface active layer (1 to 5 m thick) is unfrozen during summer. It often consists of large blocks with air voids and the bottom part of this blocky layer sometimes contains finer and wetter particles. In scree slopes and moraine deposits, the fine material is usually more abundant in the active layer. Permafrost *sensu stricto* can be found below this layer; it has a thickness of a few metres to several tens of metres in the Alps. The upper part of the permafrost body is expected to contain more massive ice, especially in rock glaciers with relatively low temperatures (Haeberli *et al.* 1998), than the lower levels, where the ground is only saturated or under-saturated with ice and the temperature is close to 0°C. Unfrozen materials are also likely to be met within the permafrost body (Vonder Mühll 1992). Finally, an abrupt transition from overlying sediments, which could be frozen and saturated with ice, to the bedrock is also to be expected. In the Alps, the spatial distribution of permafrost is generally discontinuous and, moreover, the ice distribution in the frozen ground is far from being homogeneous (Haeberli 1985).

The electrical resistivity survey is a particularly suitable method for investigating the stratigraphy of unconsolidated frozen materials in permafrost areas and for characterizing different types of ground ice (Vonder Mühll 1993; Haeberli and Vonder Mühll 1996). Because of the high resistivity of frozen sediments, geoelectrical methods can distinguish, with satisfactory accuracy, frozen from unfrozen materials.

## INSTRUMENTATION AND SURVEY DESIGN

The surveys were undertaken using a Sting/Swift (Advanced Geosciences Inc.) imaging system. The main parts of this multi-electrode system are a resistivity meter, a switching unit, three electrode cables (14 electrodes per cable) and a 12-volt external battery. We used an output voltage of 400 V. A specific electrode device was designed. Steel stakes 1-m long were driven into the surface layer interstices as deeply as possible to try to get contact with the sparse fine particles accumulated at depth. We attached sponges soaked in salt water in order to improve galvanic coupling (Fig. 2). Nevertheless, ground contact resistance was high (about 80 kΩ) and only a weak current could be injected (about 5 mA). Fortunately, there were no noticeable disturbances (telluric currents, man-made noise) that could produce spurious data and thereby inhibit reasonable interpretation. The few bad data points were easily removed from the data sets.

FIGURE 2
The typical surface of a rock glacier is composed of large blocks with air voids. Long steel stakes and sponges soaked in salt water are used to inject current into the ground.

The surveys were carried out using a Wenner-Schlumberger array. The sensitivity patterns for various electrode arrays can be evaluated for a homogeneous earth using the Frechet derivatives (McGillivray and Oldenburg 1990; Loke and Barker 1995). The Wenner-Schlumberger array is a hybrid between the Wenner and Schlumberger arrays and is moderately sensitive to both horizontal and vertical structures. As both types of geological structure can be expected in permafrost studies, the Wenner-Schlumberger array may be a good compromise between the dipole-dipole and the Wenner arrays that are sensitive to vertical and horizontal structures, respectively. We used a 10-m electrode spacing at the Verbier site and a 5-m electrode spacing at the Creux du Van site. The electrodes locations and the topography were measured using a differential global positioning system (dGPS).

## THE INVERSION AND DOI INDEX ALGORITHMS

### Inversion

The inversion of the resistivity data was carried out using the 2D inversion program RES2DINV (Loke and Barker 1996; Loke and Dahlin 2002). A Gauss-Newton smoothness-constrained least-squares algorithm is used to determine the change in the model parameters that would minimize the sum-of-squares error between the model response and the observed data values (Lines and Treitel 1984; deGroot-Hedlin and Constable 1990; Loke and Dahlin 2002). The particular inversion formulation used in this paper is based on the Gauss–Newton smoothness-constrained least-squares equation ($L_2$-norm) with the Marquardt–Levenberg modification (Lines and Treitel 1984; Ellis and Oldenburg 1994). This formulation is further modified to incorporate weighting matrices and to correspond to the Farquharson and Oldenburg (1998) formulation:

$$\left(\mathbf{J}_\mathbf{k}^\mathrm{T}\mathbf{R}_\mathrm{d}\mathbf{J}_\mathbf{k}+\lambda_k\mathbf{F}_\mathrm{R}\right)\Delta\mathbf{q}_\mathbf{k} = \mathbf{J}_\mathbf{k}^\mathrm{T}\mathbf{R}_\mathrm{d}\mathbf{g}_\mathbf{k}-\lambda_k\mathbf{F}_\mathrm{R}\left(\mathbf{q}_{\mathbf{k}-1}-\mathbf{q}_0\right), \quad (1)$$

$$\text{with} \quad \mathbf{F}_\mathrm{R} = \alpha_s\mathbf{R}_\mathbf{s}+\alpha_x\mathbf{C}_\mathbf{x}^\mathrm{T}\mathbf{R}_\mathbf{x}\mathbf{C}_\mathbf{x}+\alpha_z\mathbf{C}_\mathbf{z}^\mathrm{T}\mathbf{R}_\mathbf{z}\mathbf{C}_\mathbf{z}, \quad (2)$$

where $\Delta\mathbf{q}_\mathbf{k}$ is the change in the model parameters for the iteration $k$, $\mathbf{q}_{\mathbf{k}-1}$ is the model parameter vector (the logarithms of the model resistivity values) at the iteration $k$-1, $\mathbf{q}_0$ is a homogeneous half-space reference model, $\mathbf{g}_\mathbf{k}$ is the discrepancy vector, the difference between the logarithms of the measured and calculated apparent resistivity values. $\mathbf{R}_\mathbf{d}$, $\mathbf{R}_\mathbf{x}$, $\mathbf{R}_\mathbf{z}$ and $\mathbf{R}_\mathbf{s}$ are weighting matrices introduced so that different elements of the data misfit and model roughness vectors can be weighted, $\mathbf{C}_\mathbf{x}$ and $\mathbf{C}_\mathbf{z}$ are the smoothing matrices in the x- and z-directions (first-

FIGURE 3
Arrangement of the model cells used in the DOI calculation and location of the data points in the apparent-resistivity pseudosection for the MF1 survey.

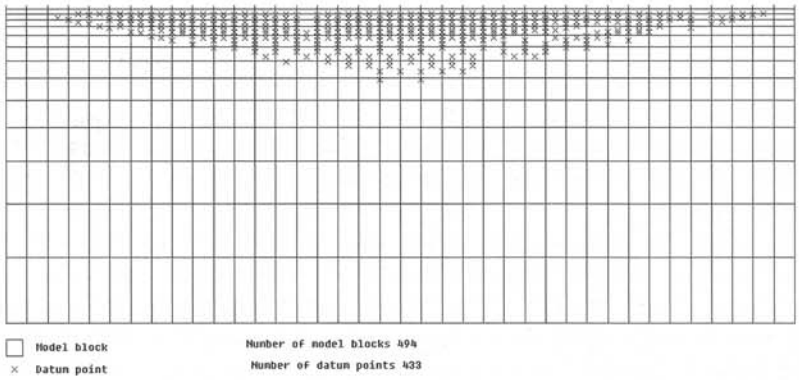


order finite-difference operators), $\alpha_s$ is a damping factor that has a value of about 0.01 to 0.0001 times the damping factors $\alpha_x$ and $\alpha_z$, $\lambda_k$ is a damping factor (Lagrange multiplier). $\mathbf{J_k}$ is the Jacobian matrix of partial derivatives, which is recalculated after each iteration. The elements of the Jacobian matrix are given by

$$J_{ij} = \frac{\partial f_i}{\partial q_j},$$

i.e. the change in the $i$th model response due to a change in the $j$th model parameter. Thus, the Jacobian matrix defines the sensitivity of measurements to changes in model parameters. The sensitivity value is a measure of the amount of information about the resistivity of a model block contained in the measured data set. If the sensitivity values of some cells become too small, the data set does not contain much information about the resistivity of these cells. This could occur in regions of the subsurface with high resistivity contrasts.

The inversion was carried out to the point at which the difference between consecutive root-mean-square (rms) errors was less than 5%. This value normally indicates that the inversion process has converged. Since the data rms misfit usually converges to approximately the amount of random noise in the measured apparent resistivities, we assumed 2% to 5% data error. As there are no evident man-made perturbations in mountains, this noise level is mainly intended to represent measurement errors or 3D-structure effects. Assigning too great an error will result in structures being missed, and too small an error will result in model structures caused by noise rather than by real ground structures. This aspect cannot be over-emphasized. Moreover, with synthetic data from models with high resistivity contrasts, Olayinka and Yaramanci (1999) showed that the best model is frequently the inverted model at a relatively low iteration number. In the field surveys presented below, convergence occurred after a maximum of 5 iterations. A finite-element calculation is used in RES2DINV for the forward problem, and topography can be included in the computation using a distorted finite-element mesh (Loke 2000).

**DOI index calculation**

The depth of investigation (DOI) method proposed by Oldenburg and Li (1999) basically carries out two inversions of the same data set using different values of the reference resistivity, $\mathbf{q_0}$, in equation (1). The first reference value, $q_A$, is usually calculated from the average of the logarithm of the observed apparent resistivity values. The second reference resistivity value, $q_B$, is usually set at 10 times $q_A$. The DOI value for a model cell is given by

$$R_{AB}(x,z) = \frac{q_A(x,z) - q_B(x,z)}{q_A - q_B}. \quad (3)$$

The value of $R$ will approach zero in parts of the model where the two inversions generate the same resistivity values. In such areas, the cell resistivity is well constrained by the data. In areas where the data do not contain much information about the cell resistivity, $R$ will approach unity as the cell resistivity will be similar to the reference resistivity. This will occur at sufficiently great depths, particularly near the ends of the survey line where the data coverage is sparser. To reduce the effect of the choice of the damping factor $\alpha_s$ and the reference resistivities used, a scaled version of the DOI index was also proposed by Oldenburg and Li (1999). The depth range of the inversion model is extended to a sufficiently great depth so that the data will contain minimal information about the resistivity of the cells in the lowest layer. However, the computation time required increases as more layers are added to the inversion model. Figure 3 shows the arrangement of the model cells used in the DOI calculation, together with the location of the data points in the apparent-resistivity pseudosection for the MF1 survey data set. The horizontal position of a data point is set at the centre of the four electrodes used in the measurement, while the vertical position is set at the median depth of investigation (Edwards 1977) of the electrode configuration. This median depth of investigation is calculated using the sensitivity values for a homogeneous half-space and gives an estimate of the "depth with which a measurement of apparent resistivity on the surface can best be associated" (Barker

1989). The median depth of investigation of the largest array spacing used provides an estimate of the maximum depth of investigation of the data set. To determine the optimum depth range, we repeated the DOI calculations using models where the depth to the deepest layer ranged from about 2 to 5 times the estimated maximum depth of investigation. It was found that DOI values are greater than 0.2 (and usually much higher) at depths greater than 3 times the estimated maximum depth of investigation. According to Oldenburg and Li (1999), the DOI value increases rapidly with depth for values greater than 0.1. Thus we have chosen a depth extent of about 3.5 times the estimated maximum depth of investigation. The scaled DOI value is then calculated using the following equation:

$$R(x,z)=\frac{q_A(x,z)-q_B(x,z)}{R_M(q_A-q_B)}, \quad (4)$$

where $R_M$ is the maximum DOI value, calculated using equation (3). The scaled DOI value, calculated using the above equation is used in the following sections. The horizontal and vertical damping factors, $\alpha_x$ and $\alpha_z$, were both set to be 1.0 so that the same weights are given to horizontal and vertical structures in the inversion model. The value of $\alpha_s$ was set at 0.01 times the value of the damping factors, $\alpha_x$ and $\alpha_z$. The 'self' damping factor, $\alpha_s$, determines the degree of impact of the reference resistivity on the inversion process. It also provides some stability to the inversion process by limiting the maximum amplitude of the parameter change vector, $\Delta\mathbf{q_k}$, calculated using equation (1).

Due to the scaling, the bottom resistivities of the subsurface models might not reach the reference resistivities. The unscaled DOI values near the bottom might be as small as 0.3, but never 1.0, and the program will use this value to scale all the values (equation 4). According to Oldenburg and Li (1999), we should not place too much importance on the details in the DOI pattern with values above 0.1. The depth of investigation is indicated by the depth at which the DOI values increase rapidly, i.e. the contours are close together, and this usually occurs around the value of 0.1.

Finally, we note that a blocky (or $L_1$-norm) inversion method gives significantly better results for areas where the subsurface changes with sharp boundaries (Loke *et al.* 2001). However, we did not use an $L_1$-norm algorithm in this paper. In scaling the DOI values, the program uses the highest unscaled DOI value to scale all the values. Normally, the highest unscaled value is at the bottom, but in the case of the blocky inversion method it sometimes occurs nearer to the surface, as in our surveys, particularly where there are high resistivity contrasts with sharp boundaries. The resulting DOI maps are unable to resolve the depth of the investigation problem fully. We are presently investigating possible modifications to the DOI calculation method that might be more suitable for an $L_1$-norm-based inversion method.

**Parameters used in this paper**

To carry out DOI calculations, we need to determine the parameters of the reference model $\mathbf{q_0}$. We must decide whether the perturbed model should be more conductive or more resistive than $\mathbf{q_0}$ and which multiplication factor to choose. We must also decide whether to take differences between $\mathbf{q_0}$ and a more conductive/resistive model (this is referred to as a one-sided difference) or between models that are larger and smaller than $\mathbf{q_0}$ (a two-sided difference). For a resistive target, Oldenburg and Li (1999) used a more conductive reference model with a multiplication factor between 5 to 10 and a one-sided difference. As both conductive and resistive structures (bedrock and permafrost, respectively) can be expected, we used symmetrical perturbed models with resistivities 0.1 and 10 times the background resistivity. However, we carried out some tests with extreme values for the multiplication factor (up to 100). The resulting DOI maps were very similar, with a few variations that have no real consequences for the interpretation. This low sensitivity to the multiplication factor is mainly due to the scaling of $R$.

## FIELD RESULTS

### Les Lapires test survey, Verbier area

*Site description*

A test survey was carried out at Les Lapires (2400 m a.s.l.), a large talus slope near Mt Gelé (Verbier area, western Swiss Alps). The surface of the talus slope is composed of blocks of metamorphic origin (gneiss, schists, amphibolites, prasinites) and presents various landforms, which can be the result of several geomorphological processes (rock falls, debris flows, permafrost creeping, soil creeping and avalanches). Geomorphological observations, together with surface and ground temperature measurements, give some clues as to the presence of discontinuous permafrost under the scree (Reynard *et al.* 1999). In 1998, during the construction of a cable-car, crossing the scree slope, ground ice was found.

*Results*

Measurements were carried out to investigate and improve the potential of 2D electrical resistivity imaging under the conditions described above. Two electrical-imaging profiles were carried out near pole 9 on the lower part of the slope, where frozen ground was suspected (Fig. 4). Although the two profiles are presented on the same figure, they were separately inverted. The test survey was carried out with one

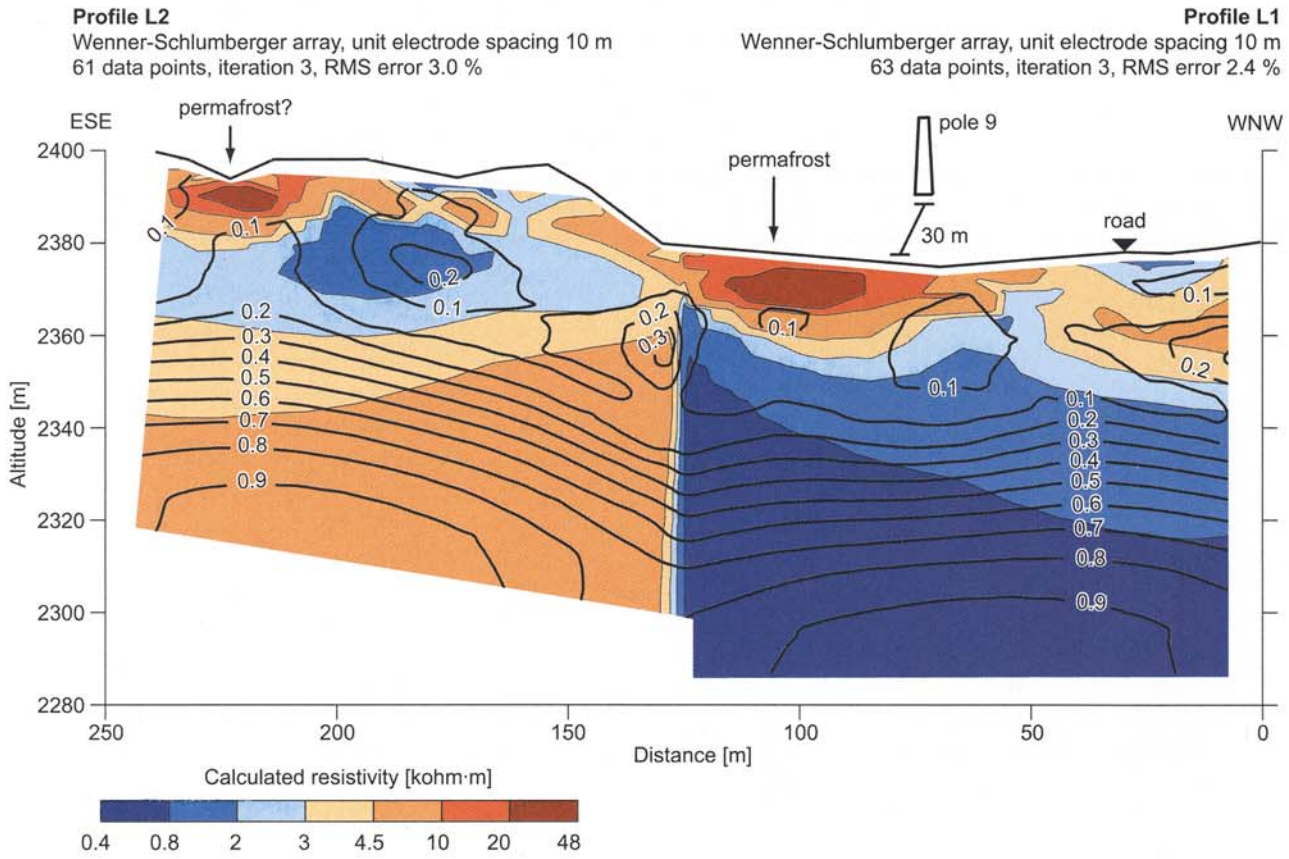


FIGURE 4

Profile L1 (from 0 to 130 m) and profile L2 (from 130 to 250 m) at Les Lapires (Verbier area). The inverted profiles are shown with their DOI indexes computed using different reference backgrounds. The contour interval is 0.1. Note that the DOI index map removes the artefacts at depth (conductive/resistive bedrock).

single 14-electrode cable and is not a real roll-along profile. Profiles L1 and L2 converged after 3 iterations with residual rms errors lower than 5%. The reference models for profiles L1 and L2 were half-spaces of 3.825 kΩm and 2.947 kΩm, respectively. Due to the different reference models, strong artefacts appear at depth. At the bottom of profile L2, the bedrock appears more resistive than on profile L1. The DOI curves were computed using symmetrical perturbed models with resistivities 0.1 and 10 times the background resistivity. Interpreting the model with a first cut-off of $R = 0.1$ (Oldenburg and Li 1999) and a contour space value of 0.1, leads to the following observations. We note that a continuous $R = 0.1$ value is at a depth of about 30 m on profile L1 and 40 m on profile L2. The DOI curve for $R = 0.9$ approaches 70 m on both profiles. Once the DOI index begins increasing, it determines precisely the depth below which the data are no longer sensitive to the earth model. Plotting the DOI curves on the resistivity profiles removes almost entirely the artefacts at depth, thus providing a coherent image of the subsurface. Areas with DOI values higher than 0.1 are present within both models. These zones are closely related to the resistive structures or are located at the extremities of the profiles. A good example of a low sensitivity area can be observed on the eastern part of profile L2, beneath the resistive structure. As a result, little reliable information about the bedrock immediately under this frozen body can be obtained.

Profile L1 shows a relatively resistive zone (between 10 to 20 kΩm) beneath the 80 metres distance mark. This structure may be attributed to permafrost with low ice content such as the one observed during the construction of pole 9. An area of higher resistivity (over 20 kΩm) can be identified within the eastern part of the profile and appears to contain more ice. The latter area coincides with the part of the slope where the ground temperature during the height of winter is the lowest (Delaloye, Reynard and Lambiel 2000. Pergélisol et construction des remontées mécaniques : l'exemple des Lapires (Mont-Gelé, Valais), unpublished report). Towards the base of profile L1, a relatively conductive layer (lower than 3 kΩm) can be identified. This layer is thought to be the unfrozen bedrock composed of gneissic rocks. As we used a 10-m electrode

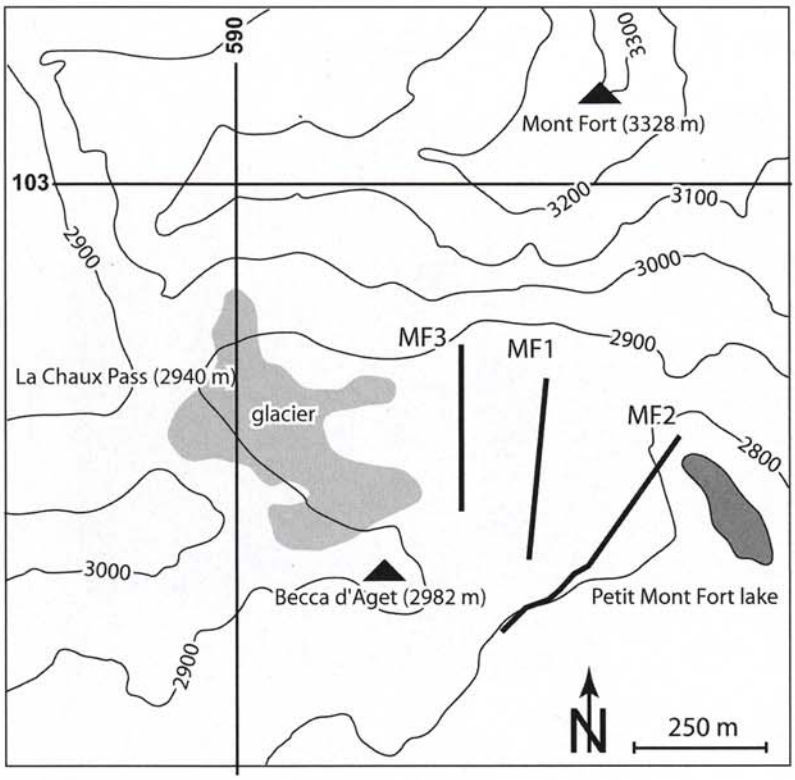


FIGURE 5
Locations of MF1, MF2 and MF3 profiles in the Verbier (Swiss Alps) area.

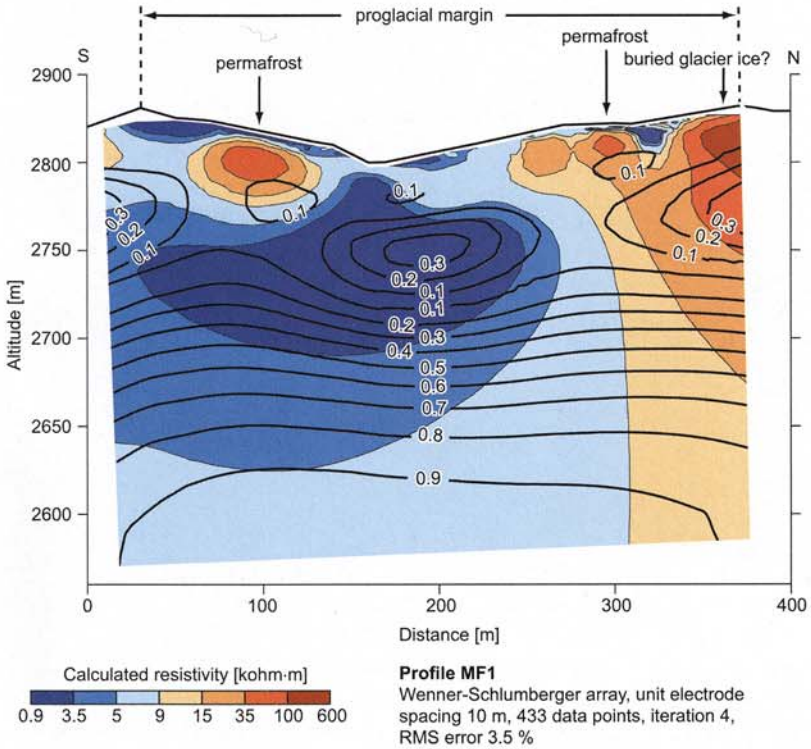


FIGURE 6
Profile MF1 at Mont Fort (Verbier area) with the DOI index map. The contour interval is 0.1. A cut-off value lower than 0.1 may be needed on the northern part of the profile.

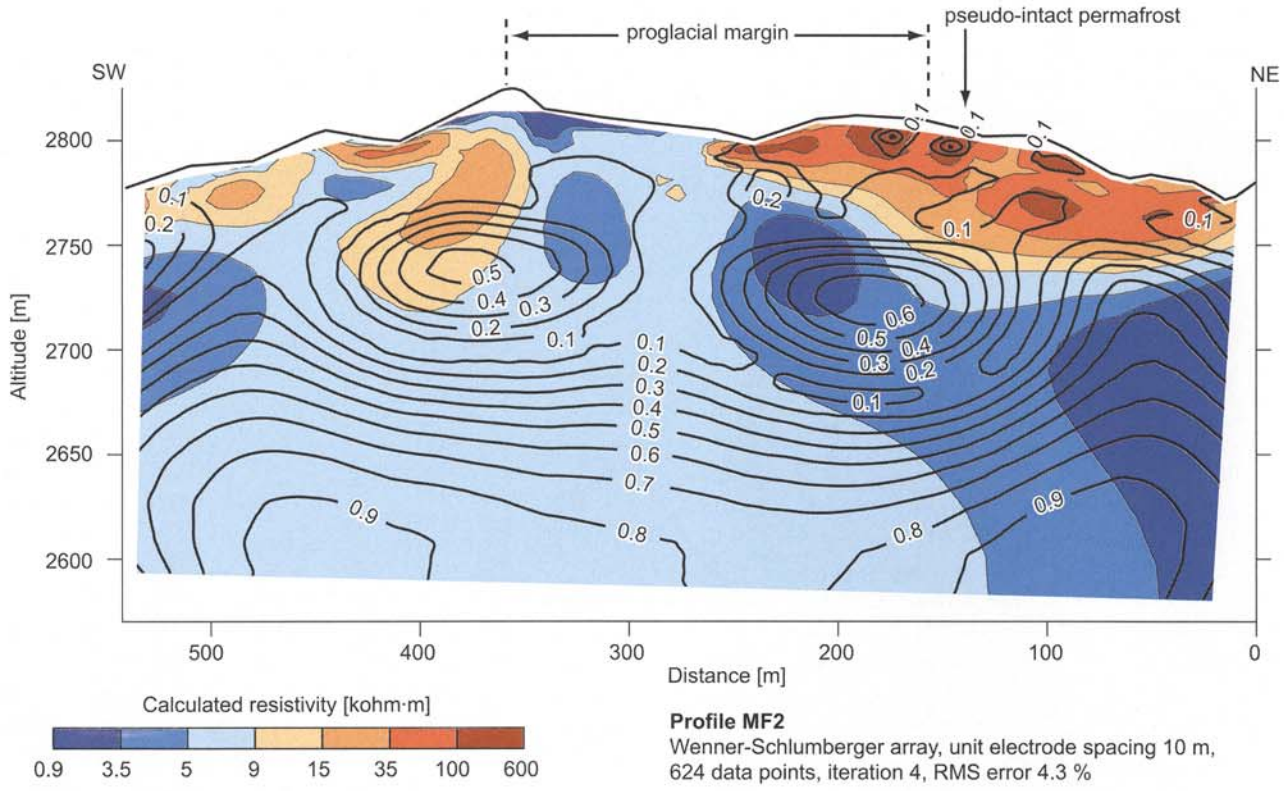


FIGURE 7

Profile MF2 at Mont Fort (Verbier area) with the DOI index map. The contour interval is 0.1. Note the high DOI value beneath the resistive structures.

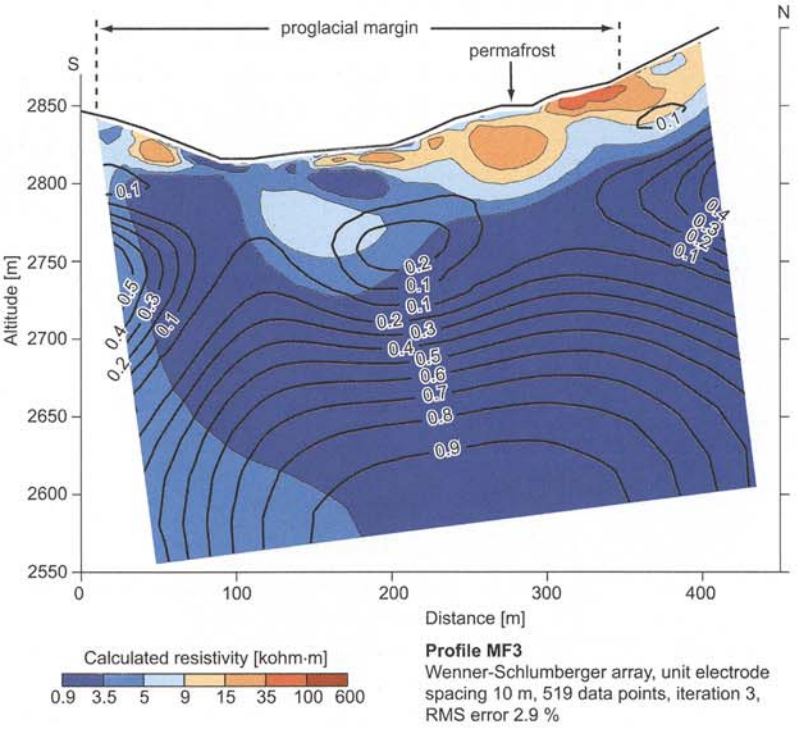


FIGURE 8

Profile MF3 at Mont Fort (Verbier area) with the DOI index map. The contour interval is 0.1. The bedrock appears less resistive than on profiles MF1 and MF2.

spacing, the thin active surface layer (< 5 m thick) cannot be observed. Profile L2 crosses a relict rock glacier (note the different topography) and confirms the absence of ice suspected in this landform. On the eastern part of this profile, resistive material can be observed again which corresponds at the surface to gelifluction lobes. The heterogeneous nature of the resistivity distribution (between 4 and 15 kΩm) within the two profiles indicates that material possessing various characteristics, possibly slightly frozen, is present in the scree slope.

**The Mont Fort survey, Verbier area**

*Site description*

The second survey was conducted on the historical proglacial margin of a small glacier (the Becca d'Agè glacier, 2800 m a.s.l.) near Mont Fort. The Becca d'Agè glacier partially overlaid and destroyed an active rock glacier during the Little Ice Age. This overlying is assumed to have resulted in thermal degradation as well as in a mechanical displacement (push-moraine, for the definition see Haeberli 1979) of the pre-Little Ice Age active rock glacier. Electrical resistivity imaging was used here to give an insight into the degradation of the permafrost in the proglacial margin and to detect pseudo-intact permafrost and buried glacier ice, which could be found on the borders of this proglacial margin. In the region, gneissic rocks dominate the geology.

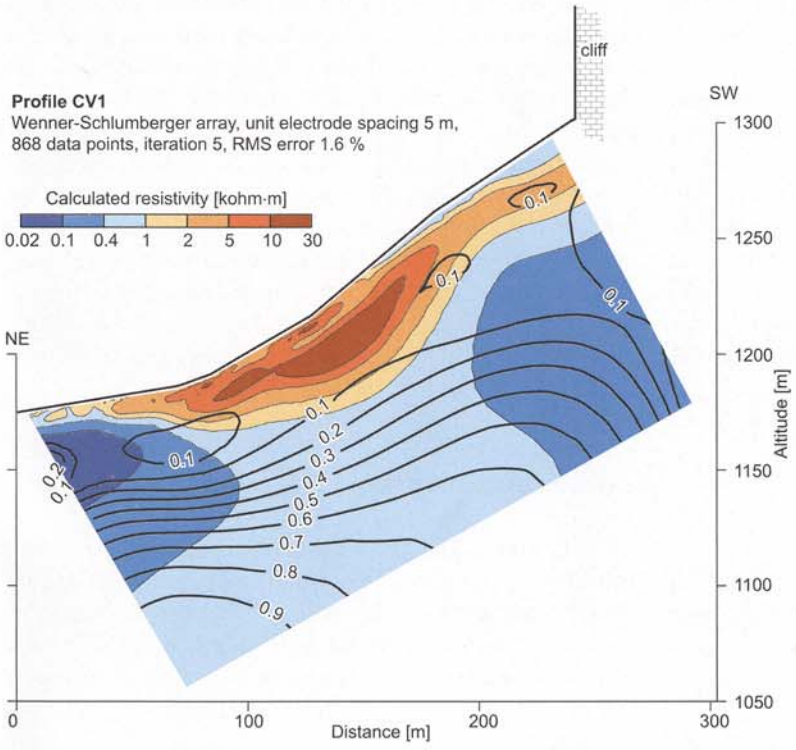


FIGURE 9

Profile CV1 at the Creux du Van (Jura Mountains) with the DOI index map. The contour interval is 0.1. The area of higher resistivity suggests that the ground is permanently frozen.

*Results*

Three transverse profiles (Figs 5, 6, 7 and 8) were recorded through the historical proglacial margin of the Becca d'Agè glacier and on the pseudo-intact part of the rock glacier. The three profiles converge after 3 or 4 iterations with an rms error lower than 5%. The reference models for profiles MF1, MF2 and MF3 were half-spaces of 6.846 kΩm, 13.626 kΩm and 5.961 kΩm, respectively. The DOI curves were computed using symmetrical perturbed models with resistivities 0.1 and 10 times the background resistivity. As can be observed on the figures, the DOI maps depend significantly on the overlying resistive structures. Areas with DOI contour values higher than 0.1 appear immediately beneath the resistive structures (> 35 kΩm); for example, examine the NE side of profile MF2. In addition, a series of artefacts occurs along the three profiles. On profile MF2, the large resistive anomaly between distances 340 and 430 may not extend to an altitude of about 2750 m. It appears that this structure is not necessarily indicated by the data at depth. The same conclusion can be drawn for profile MF3 with the resistive structure beneath the proglacial margin. Moreover, the resistivity of buried glacier ice cannot be accurately determined ($R$>0.1 for resistivity structures over 100 kΩm), although using a cut-off value of 0.1 appears to work well with most data sets. Nevertheless, a lower cut-off value (e.g. 0.05) might be needed on profile MF1 since the vertical resistive structure (beneath the 280 m mark, altitude 2760 m) within the northern part of the profile is geologically not plausible.

On the three profiles, the central depressed part of the proglacial margin shows relatively low resistivities (< 9 kΩm) in the uppermost layers, which probably means that permafrost does not occur here and could have been thawed by the glacier advance. On each side of the proglacial margin, more resistive structures (>15 kΩm) are identified as permafrost bodies that were not completely degraded by the glacier advance. On the northern side of profile MF1, patches of very high resistivity terrain (>300 kΩm) could be interpreted as buried dead glacier ice. This theory is reinforced by the presence of a thermokarst depression (thaw of massive ice) occurring near the northern extremity of MF1.

**The Creux du Van survey, Jura Mountains**

*Site description*

The Creux du Van, the third site investigated, is located in the Jura Mountains (north-western Switzerland). The north-

orientated talus slope of the site has developed beneath a 150-m high limestone cliff thus greatly reducing significant solar radiation. The upper part of the slope is generally free of vegetation whereas the lower scree slope is covered with alpine trees and mosses. Abnormally small dwarf spruces are found in a few glades on the lower part of the slope, whereas the subsurface temperature shows a strong negative anomaly. This is, in the absence of a microclimate at the Creux du Van, an indication of the presence of very cold ground conditions. Despite the low altitude (1200 m a.s.l., mean annual air temperature is +5.5°C), the occur-rence of permafrost (at a temperature of about 0°C) is mainly due to complex air circulation through the whole scree slope (Delaloye and Reynard 2001).

*Results*

A profile (CV1) was recorded along the whole slope (Fig. 9). This profile converged after 5 iterations with a very low rms error (< 2%). This low rms error could be due to the exceptionally good quality of the data and also to the probable 2D-shape of the structures. The reference model for profile CV1 was a half-space of 2.178 kΩm. The DOI curves were computed using symmetrical perturbed models with resistivities 0.1 and 10 times the background resistivity.

At the bottom mid-section of the slope, the survey line crossed a glade with small trees where frozen ground was suspected. An area of higher resistivity (5 to more than 20 kΩm) can be identified and suggests that ice is present. At the bottom of the slope, more conductive underlying marls (< 0.4 kΩm) can be observed on the profile, overlain by heterogeneous moraine from the last glacial epoch (0.4 to 2 kΩm). The upper part of the slope is composed of rock debris (5 to 2 kΩm). The DOI map indicates that the marls at the bottom of the slope need not be enclosed and can still exist beneath the scree slope. The bottom of the permafrost probably overlies the more conductive marls at depth. According to the DOI map, the upper part of the survey is still sensitive to a low resistivity zone at depth (about 0.4 kΩm).

## CONCLUSIONS

This study has enabled us to improve or confirm our understanding of the subsurface structures at three different sites. The effectiveness of 2D resistivity imaging is proven despite unfavourable contact resistance due to the presence of large surface blocks with voids. With this technique, ice can be located with sufficient accuracy for geotechnical investigations. Electrical imaging gives a good image of the permafrost structures. However, as can be deduced from the DOI calculations, little reliable information about the bedrock can be obtained immediately under the massive ice and we cannot determine the resistivity within the high resistivity zones (over 100 kΩm) accurately. At Les Lapires, the permafrost beneath the cable-car pole is well imaged and the resistivity distribution within the two profiles determines the thermal heterogeneity of the material present in the scree slope (Fig. 4). The Mont Fort surveys (Figs 5, 6, 7 and 8) show that the pre-Little Ice Age active rock glacier was partly degraded during the progression of the Becca d'Agè glacier, whereas pseudo-intact permafrost is still present at the margins of the proglacial area. Finally, resistivity imaging gave valuable information about the structure of the Creux du Van low-altitude permafrost (Fig. 9).

In subsurfaces with heterogeneous high resistivity features, DOI maps are expressly required to determine the areas where, and the depth below which, the data are no longer sensitive to the electrical properties of the earth. Without DOI maps, interpretation of such models is difficult, non-representative and dangerous. To process DOI maps, we used two-sided perturbed models with resistivities 0.1 and 10 times the background resistivity, as both conductive and resistive structures can be expected. We also used a scaled DOI index, making DOI maps less sensitive to the choice of the multiplication factor. Using a cut-off value of 0.1 appears to work well with most data sets but a lower cut-off value might be needed on some profiles. As can be deduced from the field examples, the DOI maps prevent over-interpretation or misinterpretation of inversion results in permafrost and rock glacier studies. The DOI map helps to explain the occurrence of erratic and non-geological structures at depth. It also defines the depth to which we can investigate in an inverted resistivity profile. In the near future, the use of DOI maps should become an essential tool for reliable interpretation of all 2D and 3D resistivity and IP imaging surveys.

## ACKNOWLEDGEMENTS

M.H.L. acknowledges the support provided by the School of Physics, Universiti Sains Malaysia. The authors are greatly indebted to L. Baron and R. Monnet (University of Lausanne) for their valuable help during the field surveys. The authors are also grateful to two anonymous reviewers for their useful comments that have assisted in improving this paper.

## REFERENCES


Barker R.D. 1989. Depth of investigation of collinear symmetrical four-electrode arrays. *Geophysics* **54**, 1031-1037.

Barsch D. 1996. *Rockglaciers. Indicators for the Present and the Former Geoecology in High Mountain Environments.* Springer Verlag, Berlin/Heidelberg.

deGroot-Hedlin C. and Constable S. 1990. Occam's inversion to generate smooth, two-dimensional models from magnetotelluric data. *Geophysics* **55**, 1613-1624.

Delaloye R. and Devaud G. 2000. La distribution du pergélisol dans les marges proglaciaires des glaciers de Challand, d'Aget et du Sanetschhorn (Valais, Alpes Suisses). In: Hegg, Ch., Vonder Mühll (Hrsg.), Beiträge zur Geomorphologie. Proceedings der Fachtagung der Schweizerischen Geomorphologischen Gesellschaft vom 8.-10. Juli in Bramois (Kt. Wallis). Birmensdorf, Eidg. Forschungsanstalt WSL, 87-96.

Delaloye R. and Reynard E. 2001. Les éboulis gelés du Creux du Van (Chaîne du Jura, Suisse). *Environnements périglaciaires, Bulletin de l'Association Française du Périglaciaire* **8**, 118-129.

Edwards L.S. 1977. A modified pseudosection for resistivity and induced-polarization. *Geophysics* **42**, 1020-1036.

Ellis R.G. and Oldenburg D.W. 1994. Applied geophysical inversion. *Geophysical Journal International* **116**, 5-11.

Farquharson C.G. and Oldenburg D.W. 1998. Non-linear inversion using general measures of data misfit and model structure. *Geophysical Journal International* **134**, 213-227.

Haeberli W. 1979. Holocene push-moraine in Alpine permafrost. *Geographiska Annaler* **61** A (1-2), 43-48.

Haeberli W. 1985. Creep of mountain permafrost: internal structure and flow of alpine rock glaciers, *Mitteilungen der Versuchsanstalt fuer Wasserbau, Hydrologie und Glaziologie - ETH Zürich* **77**.

Haeberli W. 1992. Construction, environmental problems and natural hazards in periglacial mountain belts. *Permafrost Periglacial Processes* **3**, 111-124.

Haeberli W., Guodong C., Gorbunov A. P. and Harris S. A. 1993. Mountain permafrost and climatic change. *Permafrost Periglacial Processes* **4**, 165-174.

Haeberli W., Hoelzle M., Kääb A., Keller F., Vonder Mühll D. and Wagner S. 1998. Ten years after drilling through the permafrost of the active rock glacier Murtèl, eastern Swiss Alps: answered questions and new perspectives. Proceedings 7th International Conference on Permafrost ,Yellowknife, Canada, 403-410.

Haeberli W., Kääb A., Hoelzle M., Bösch H., Funk M., Vonder Mühll D. and Keller F. 1999. Eisschwund und Naturkatastrophen im Hochgebirge. Schlussbericht NFP 31, Vdf Hochschulverlag, ETH Zurich.

Haeberli W. and Vonder Mühll D. 1996. On the characteristics and possible origins of ice in rock glacier permafrost. *Zeitschrift für Geomorphologie N.F., Suppl. Bd.* **104**, 43-57.

Harris C., Davies M. C. R. and Etzelmüller B. 2001. The assessment of potential geotechnical hazards associated with mountain permafrost in a warming global climate. *Permafrost Periglacial Processes* **12**, 145-156.

Hauck C. 2001. Geophysical methods for detecting permafrost in high mountains. *Mitteilungen der Versuchsanstalt fuer Wasserbau, Hydrologie und Glaziologie - ETH Zürich* **171**.

Hauck C. and Vonder Mühll D. 1999. Using DC Resistivity Tomography to Detect and Characterise Mountain Permafrost. 61st EAGE Conference, Helsinki, Finland, Extended Abstracts, 2-15.

Kneisel C. 1999. Permafrost in Gletschervofeldern. Eine vergleichende Untersuchung in den Ostschweizer Alpen und Nordschweden. *Trierer Geographische Studien* **22**.

Kneisel C., Hauck C. and Vonder Mühll D. 2000. Permafrost below the timberline confirmed and characterized by geoelectrical resistivity measurements, Bever Valley, Eastern Swiss Alps. *Permafrost Periglacial Processes* **11**, 295-304.

Lines L.R. and Treitel S. 1984. Tutorial : A review of least-squares inversion and its application to geophysical problems. *Geophysical Prospecting* **32**, 159-186.

Loke M.H. 2000. Topographic modelling in resistivity imaging inversion. 62nd EAGE Conference, Glasgow, UK, Extended Abstracts, D-2.

Loke M.H., Acworth I. and Dahlin T. 2001. A comparison of smooth and blocky inversion methods in 2-D electrical imaging surveys. 15th ASEG Conference & Technical Exhibition, Brisbane, Extended Abstracts.

Loke M.H. and Barker R.D., 1995. Least-squares deconvolution of apparent resistivity pseudosections. *Geophysics* **60**, 1682-1690.

Loke M.H. and Barker R.D. 1996. Rapid least-squares inversion of apparent resistivity pseudosections using a quasi-Newton method. *Geophysical Prospecting* **44**, 131-152.

Loke M.H. and Dahlin T. 2002. A comparison of the Gauss-Newton and quasi-Newton methods in resistivity imaging inversion. *Journal of Applied Geophysics* **49**, 149-162.

Maisch M., Wipf A., Denneler B., Battaglia J. and Benz C. 1999. Auswirkungen von Klimaänderungen auf die Gletscher und deren Vorfelder. Schlussbericht NFP 31. Vdf Hochschulverlag an der ETH Zürich.

Marescot L., Monnet R., Baron L., Lambiel C., Reynard E., Delaloye R. and Chapellier D. 2001. 2D electrical resistivity imaging in mountain permafrost studies: three challenging surveys in the Swiss Alps and Jura Mountains. Proceedings of the 7th EEGS-ES meeting, Birmingham, England, pp. 104-105.

McGillivray P.R. and Oldenburg D.W. 1990. Methods for calculating Frechet derivatives and sensitivities for the non-linear inverse problem: A comparative study. *Geophysical Prospecting* **38**, 499-524.

Olayinka A.I. and Yaramanci U. 1999. Choice of the best model in 2-D geoelectrical imaging: case study from a waste dump site. *European Journal of Environmental and Engineering Geophysics* **3**, 221-244.

Oldenburg D.W. and Li Y. 1999. Estimating depth of investigation in dc resistivity and IP surveys. *Geophysics* **64**, 403-416.

Reynard E., Delaloye R. and Lambiel C. 1999. Prospection géoélectrique du pergélisol alpin dans le massif des Diablerets (VD) et au Mont Gelé (Nendaz, VS). *Bulletin de la Murithienne* **117**, 89-103.

Roy A. 1972. Depth of investigation in Wenner three-electrode and dipole-dipole dc resistivity methods. *Geophysical Prospecting* **20**, 329-340.

Roy A. and Apparao A. 1971. Depth of investigation in direct current methods. *Geophysics* **36**, 943-959.

Vonder Mühll D. 1992. Evidence of intrapermafrost groundwater flow beneath an active rock glacier in the Swiss Alps. *Permafrost Periglacial Processes* **3**, 169-172

Vonder Mühll D. 1993. Geophysikalische Untersuchungen in Permafrost des Oberengadins. *Mitteilungen der Versuchsanstalt fuer Wasserbau, Hydrologie und Glaziologie - ETH Zürich* **122.**

Vonder Mühll D., Hauk C., Gubler H., McDonald R. and Russill N. 2001. New geophysical methods of investigating the nature and distribution of mountain permafrost with special reference to radiometry techniques. *Permafrost Periglacial Processes* **12**, 27-38.